Model-Independent Quantification of Complex Shear Modulus via Speed and Attenuation of Surface Waves

Bhaskara Rao Chintada, Richard Rau, Orcun Goksel
Computer-assisted Applications in Medicine, ETH Zurich, Switzerland

***Abstract*—Shear-wave elastography imaging has been commonly used in the literature to characterize shear-wave propagation in order to estimate shear modulus in soft tissues. Instead of bulk shear waves, waves in thin tissue structures such as the layers of skin or membranes of organs travel following surface wave characteristics. Biomechanical characterization of surface waves in the literature often utilized model-based approximations for propagation speed, thereby omitting the effects of surface wave attenuation. In this work, we propose a method to estimate complex shear modulus from surface waves using both phase velocity and attenuation. We demonstrate this to estimate complex shear modulus of the skin at four different locations in upper extremity. For this purpose, we induce surface waves using a piezoelectric shaker on the skin, actuated at 25 Hz. Surface waves are tracked with high-frame rate plane-wave imaging using a high-frequency L22-14v transducer. We found an average storage-to-loss moduli ratio of 1.10, indicating that the loss modulus plays a significant role for the characterization of the skin and thus should not be ignored as common in the literature.**

***Index Terms*—Ultrasound, Tissue biomechanics, Skin.**

I. INTRODUCTION

Surface Wave (SW) elastography methods are developed to measure superficial soft tissue elastic characteristics in thin (slab) tissue structures (e.g., the skin, heart wall, organ capsules, membranes, etc.). Conventionally, surface waves are induced by an external exciter, and their propagation is observed using ultrasound imaging to capture the lateral surface wave travel speed. SW methods are similar to Shear-wave Elastography Imaging (SWEI) methods used to map shear-wave speed (SWS) in bulk media, e.g., soft tissues. SWS has been studied in many clinical applications including diagnosis of diseases in liver, breast and kidney [1]–[3]. However, SWS has shown low specificity in breast cancer diagnosis [4] and in the early-stage diagnosis of nonalcoholic fatty liver disease (NAFLD) [5], [6] as soft tissues are inherently viscoelastic [7]. With this motivation, several complementary bio-markers have been proposed to characterize tissue viscoelasticity [8], [9]. To fully characterize viscoelasticity of soft tissue storage $G'(\omega)$ and loss $G''(\omega)$ moduli at frequency ω is required. Using SWEI methods, these moduli can be derived from shear-wave phase velocity and attenuation (i.e., the decay of shear-wave amplitude with distance) [10]–[13].

Complex shear modulus can facilitate a comprehensive characterization of soft issues. Real part of complex modulus is known as the storage modulus, and has been studied extensively as a biomarker for diagnosis and disease staging. However, conventional SW approaches often utilize shear storage modulus derived based on the propagation speed of the surface wave, typically using model-based approximations while omitting the influence of surface-wave attenuation [14]–[16]. It is, however, known from recent SWEI methods in bulk media that the shear attenuation and shear loss modulus can be used as additional bio-markers. For example, loss modulus improves differential diagnosis of liver tumors than the storage modulus [17], and shear attenuation was shown to enhance sensitivity in the segregation of transplanted livers for rejection [18].

Characterization of SW attenuation and loss modulus may add complementary information in early diagnosis and staging of, e.g., skin diseases such as fibrosis as an early sign of systemic sclerosis. In this work, we introduce methods to compute shear wave attenuation and model-independent complex moduli from surface wave speed and attenuation values. We exemplify our approach by measuring complex shear moduli values of different regions of the skin.

II. MATERIALS AND METHODS

A. Data acquisition

A piezoelectric actuator was used to generate a surface wave travelling on the skin. Surface wave propagation is then tracked with ultrasound imaging, using ultrasound gel as a coupling medium, cf. Fig. 1. We employed ultrafast ultrasound imaging at 10 k frames-per-second and coherent compounding of three plane waves at {-8°,0°,8°} with a moving-average compounding of latest 3 frames. This acquisition sequence was programmed on a research ultrasound machine (Verasonics, Seattle, WA, USA) for a 128-element linear-array transducer (L22-14v) operating at 16 MHz center frequency. The SW propagation is tracked using a 2D Loupas autocorrelation method [19] along the depth axis z, leading to particle velocity profiles $\dot{u}(r,t)$, where r is the propagation distance and t the time.

B. Surface wave displacements

Several modes of SW displacement fields can be expressed as [20]:

$$U_m(r,\omega) = \sum_m A_m(r,\omega) e^{i(\omega t - k_m(\omega) r)} \tag{1}$$

978-1-7281-5448-0/20/$31.00 ©2020 IEEE

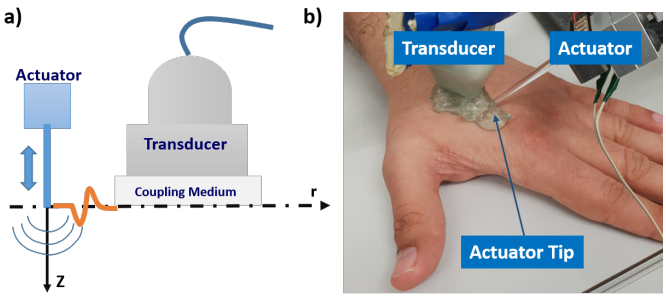

Fig. 1. (a) Schematic of surface wave generation and detection on the skin (b) Sample experimental setup.

where ω is the angular frequency, $k_m(\omega)$ is the wave-number, and $A_m(r,\omega)$ is the amplitude of m^{th} mode of surface waves.

When we induce the surface waves using an actuator on a surface as shown in Fig. 1a, $A_m(r,\omega)$ can then be expressed as a function of input source and propagation distance r as:

$$U_m(r,\omega) = \sum_m I(\omega)R_m(\omega)\frac{e^{-\alpha_m(\omega)}}{\sqrt{r}}e^{i(\omega t - k_m(\omega)r + \phi_o(\omega))}. \tag{2}$$

where $I(\omega)$ is the amplitude spectrum of the source, $R_m(\omega)$ is the soft tissue response, $\alpha_m(\omega)$ is the intrinsic attenuation for the m^{th} mode of surface wave, $\sqrt{r}$ is the diffraction factor and $\phi_o(\omega)$ is the phase spectrum of the source. Considering a single mode of surface wave and with the intrinsic attenuation α_r and wave-number k_r, the above can be rewritten as:

$$U(r,\omega) = I(\omega)R(\omega)\frac{e^{-\alpha_r(\omega)}}{\sqrt{r}}e^{i(\omega t - k_r(\omega)r + \phi_o(\omega))}. \tag{3}$$

Separating this complex equation into amplitude ($|U(r,\omega)|$) and phase components ($\angle U(r,\omega)$), and taking the logarithm of the former component on both sides, we arrive at:

$$\ln(|U(r,\omega)|) = -\alpha_r(\omega)r - \frac{1}{2}\ln(r) - \ln(I(\omega)R(\omega)), \tag{4a}$$

$$\angle U(r,\omega) = -\left[\frac{\omega}{c_r(\omega)}\right]r - \theta_0\,. \tag{4b}$$

We herein use Eq. (4) to compute the intrinsic surface wave attenuation by solving it for $\alpha_r(\omega)$ in a least-square sense by using values (i.e., $-\ln\|U(r,\omega)\| - \frac{1}{2}\ln(r)$) at different propagation distances r. Similarly, we compute the frequency-dependent surface wave phase velocity $c_r(\omega)$ using phase $-\angle U(r,\omega)$ information at different propagation distances r in least-square sense.

C. Relationship between shear waves and surface waves.

Given SW phase velocity $c_r(\omega)$ and attenuation $\alpha_r(\omega)$, the complex surface wave-number $\hat{k_r}$ can be formulated as

$$\hat{k_r} = \frac{\omega}{c_r(\omega)} - i\alpha_r(\omega). \tag{5}$$

which is used herein for solving the dispersion relationship in order to derive complex shear wave-number ($\hat{k_s}$) of bulk medium. The Rayleigh wave dispersion equation in viscoelastic media mounted with a coupling medium with similar density is given by [21]:

$$4\hat{k_r}^3\beta - (\hat{k_s}^2 - 2\hat{k_r}^2) - \hat{k_s}^4 = 0. \tag{6}$$

where $\beta = \sqrt{\hat{k_r}^2 - \hat{k_s}^2}$, $\hat{k_s}$ is the shear wave-number and $\hat{k_r}$ is Rayleigh surface wave-number. This equation holds in our study case as well, as we have used ultrasound gel as a coupling medium between the ultrasound transducer and skin, as shown in the Fig. 1b. Using Eq. 6, complex shear wave-number ($\hat{k_s}$) can be computed given complex surface wave number ($\hat{k_r}$). Complex shear wave-number can be expressed in terms of shear wave phase velocity ($c_s(\omega)$) and attenuation ($\alpha_s(\omega)$) similar to Eq. 5 as

$$\hat{k_s} = \frac{\omega}{c_s(\omega)} - i\alpha_s(\omega). \tag{7}$$

D. Complex shear modulus.

In conventional SW methods to compute viscosity / loss modulus, shear-wave phase velocities at different frequencies are fitted with empirical and often heuristic mechanical models [14], Herein we present a model-independent characterization approach.

In linear, isotropic, viscoelastic media the storage $G'(\omega)$ and loss $G''(\omega)$ moduli are related to the complex shear wave-number $\hat{k_s}$ via

$$G'(\omega) + iG''(\omega) = \hat{G}(\omega) = \frac{\rho\omega^2}{\hat{k_s}^2(\omega)}, \tag{8}$$

where ρ represents the tissue density. Substituting Eq. (8) in Eq. (7) results in deriving the shear storage and loss moduli as

$$G'(\omega) = \rho\omega^2\frac{\left(\frac{\omega}{c_s(\omega)}\right)^2 - \alpha_s(\omega)^2}{\left(\left(\frac{\omega}{c_s(\omega)}\right)^2 + \alpha_s(\omega)^2\right)^2}, \tag{9a}$$

$$G''(\omega) = 2\rho\omega^2\frac{\left(\frac{\omega}{c_s(\omega)}\right)\alpha_s(\omega)}{\left(\left(\frac{\omega}{c_s(\omega)}\right)^2 + \alpha_s(\omega)^2\right)^2}. \tag{9b}$$

E. Implementation.

The induced SW particle velocity fields at depth z (i.e, $\dot{u}(z,r,t)$) by a piezoelectric actuator as shown in Fig. 1b are averaged in an axial region-of-interest (ROI). To ensure a planar wavefront, we used a 1 mm axial ROI below the skin surface at a depth of 1 mm. This then reduces the particle velocity field $\dot{u}(z,r,t)$ in the ROI to $\dot{u}(r,t) = \sum_{\text{ROI}}\dot{u}(z,r,t)$. Typical particle velocity fields tracked at different propagation distances are shown in Fig. 2 a. Note that, since particle velocity fields are just time derivatives of displacement profiles, amplitude spectrum of particle velocity fields and displacement fields are same. However, the phase spectrum of particle velocity fields shifts by 90° compared to the phase spectrum of displacement fields. Hence, we can use the Eqs. 4 to compute $c_r(\omega)$ and $\alpha_r(\omega)$ without any change using axial velocity fields instead of displacement profiles.

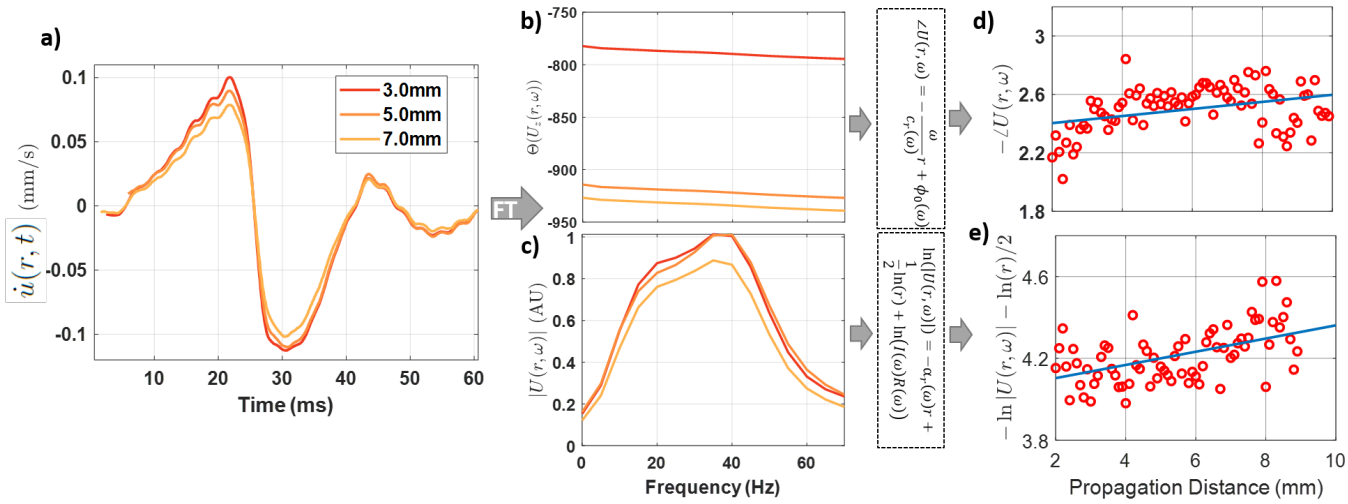

Fig. 2. Quantification of complex shear modulus: Surface wave particle velocity fields(a) its phase spectrum(b) and amplitude spectrum(c) at different lateral distances. SW phase velocity(d) and attenuation(e) estimation using Eq. 4

The 1D Fourier transform $U(r,\omega)$ of $\dot{u}(r,t)$ at different propagation distances $r_{i=1..n}$ are computed to estimate surface wave phase velocity $c_r(\omega)$ and attenuation $\alpha_r(\omega)$. Typical surface wave phase angles $\angle(U(r,\omega)$ and amplitude spectrum $|U(r,\omega)|$ at different propagation distances are shown in Fig. 2 b and c, respectively. In the next step, as per the Eq. (4), $c_r(\omega)$ and $\alpha_r(\omega)$ were obtained using the phase and amplitude profiles of $u(r,\omega)$ using 'polyfit' function in MATLAB.

The surface wave phase velocities $c_r(\omega)$ were estimated from the slope of varying $-\angle(\hat{u}(r,\omega)$ over a selected window of propagation distances as illustrated in Fig. 2d. The frequency-dependent surface wave attenuation $\alpha_s(\omega)$ is estimated as negative slope of varying surface wave amplitudes with diffraction correction (i.e., $-\ln\|U(r,\omega)\| - \frac{1}{2}\ln(r)$) as illustrated in Fig. 2e.

Calculations were performed for various combinations of start and end propagation distances to derive the best estimate of $c_r(\omega)$ and $\alpha_r(\omega)$ similar to the methods in [9]. For this purpose, while computing $c_r(\omega)$ and $\alpha_r(\omega)$ corresponding coefficient of determination (R^2) of fit was computed to evaluate goodness of the line fit. Only the estimates with R^2 greater than 0.85 were considered. Using surface wave phase velocity $c_r(\omega)$ and attenuation $\alpha_r(\omega)$, complex surface wave-number (i.e., $\hat{k_r} = \frac{\omega}{c_r(\omega)} - i\alpha_r(\omega)$) is obtained. Once we have the complex surface wave-number, complex shear wave-number (i.e., $\hat{k_s} = \frac{\omega}{c_s(\omega)} - i\alpha_s(\omega)$) can be obtained by solving the Eq. 6, from which we can derive shear wave phase velocity $c_s(\omega)$ and attenuation $\alpha_s(\omega)$.

F. Experiments

An piezoelectric exciter with sharp tip was placed next to the L22-14v transducer and pushed the skin with a pulse centred around 25 Hz. Ultrasound gel was used as a coupling medium to track the travelling surface wave. Similar, SW experiments were conducted on the #1. anterior forearm; #2. 1st dorsal interosseous muscle with thumb extended open (c.f Fig. 1b); #3. 1st dorsal interosseous muscle with thumb flexed close; and #4. dorsal to metacarpophalangeal joint (i.e., on the knuckle of the index finger). To test sensitivity to anatomical configuration, we have conducted two experiments in this region of the skin, once with the thumb open (#2) and relaxed; and once closed (#3), which makes the underneath tissue stiffer.

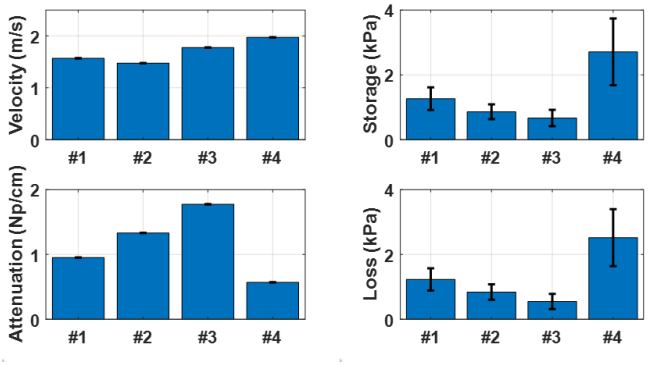

Fig. 3. (a) Shear wave phase velocity and attenuation, (b) Storage and loss moduli for different skin regions. #1. anterior forearm, #2. 1st dorsal interosseous muscle with thumb extended open (c.f Fig. 1b).#3. 1st dorsal interosseous muscle with thumb flexed close, and #4. dorsal to metacarpophalangeal joint (i.e., on the knuckle of the index finger)

III. Results and Discussion

Shear wave speed and attenuation for the skin regions #1-#4 are shown in Fig. 3a, and its corresponding shear storage and shear loss moduli are shown in Fig. 3b. #4 on-the-knuckle is seen to have the highest shear wave phase velocity with the lowest attenuation, potentially due to the superficial bone. Shear wave velocity and attenuation for #3 flexed thumb is greater than #2 relaxed thumb. These observations indicate that nearby anatomical structures and measurement position/setting

may confound biomechanical characterization via SW, and therefore need to be controlled and/or compensated. Additionally, such changes may be utilized to vary measurement settings, e.g., loading and pre-stress on tissues to estimate nonlinearity parameters similarly to [9], [22]–[24]. G' and G" values being relatively close, with their average ratio being 1.10, indicates that loss modulus plays a significant role for the skin at 25 Hz and thus cannot be ignored as typically done in the literature.

IV. CONCLUSIONS

Surface waves could be successfully generated and imaged. Surface waves were successfully quantified, in a model-independent way. Such quantifications show differentiation ability, at least with respect to anatomical location and posture affecting skin stretch. Loss modulus is found to be ≈90% of storage modulus at 25Hz, therefore should not be ignored. Surface wave quantification can become a promising diagnostic biomarker, e.g., for diseases affecting the skin, or the facia and capsules around organs.

ACKNOWLEDGEMENTS

Funding was provided by the Promedica Foundation, Chur. We also acknowledge support from the Swiss National Science Foundation.

REFERENCES

[1] A. Sarvazyan, T. Hall, M. Urban, M. Fatemi, S. Aglyamov, and B. Garra, "Elasticity imaging-an emerging branch of medical imaging. an overview," *Curr. Med. Imaging Rev*, vol. 7, no. 4, pp. 255–282, 2011.

[2] T. Deffieux, J.-L. Gennisson, L. Bousquet, M. Corouge, S. Cosconea, D. Amroun, S. Tripon, B. Terris, V. Mallet, and P. Sogni, "Investigating liver stiffness and viscosity for fibrosis, steatosis and activity staging using shear wave elastography," *Journal of Hepatology*, vol. 62, no. 2, pp. 317–324, 2015.

[3] M. Tanter, J. Bercoff, A. Athanasiou, T. Deffieux, J.-L. Gennisson, G. Montaldo, M. Muller, A. Tardivon, and M. Fink, "Quantitative assessment of breast lesion viscoelasticity: initial clinical results using supersonic shear imaging," *Ultrasound in medicine & biology*, vol. 34, no. 9, pp. 1373–1386, 2008.

[4] M. Y. Kim, N. Choi, J.-H. Yang, Y. B. Yoo, and K. S. Park, "False positive or negative results of shear-wave elastography in differentiating benign from malignant breast masses: analysis of clinical and ultrasonographic characteristics," *Acta Radiologica*, vol. 56, no. 10, pp. 1155–1162, 2015.

[5] T. Poynard, M. Munteanu, E. Luckina, H. Perazzo, Y. Ngo, L. Royer, L. Fedchuk, F. Sattonnet, R. Pais, P. Lebray *et al.*, "Liver fibrosis evaluation using real-time shear wave elastography: applicability and diagnostic performance using methods without a gold standard," *Journal of hepatology*, vol. 58, no. 5, pp. 928–935, 2013.

[6] I. Sporea, S. Bota, O. Gradinaru-Taşcău, R. Şirli, A. Popescu, and A. Jurchiş, "Which are the cut-off values of 2d-shear wave elastography (2d-swe) liver stiffness measurements predicting different stages of liver fibrosis, considering transient elastography (te) as the reference method?" *European journal of radiology*, vol. 83, no. 3, pp. e118–e122, 2014.

[7] Y.-c. Fung, *Biomechanics: mechanical properties of living tissues*. Springer Science & Business Media, 2013.

[8] C. T. Barry, B. Mills, Z. Hah, R. A. Mooney, C. K. Ryan, D. J. Rubens, and K. J. Parker, "Shear wave dispersion measures liver steatosis," *Ultrasound in Medicine & Biology*, vol. 38, no. 2, pp. 175–182, 2012.

[9] B. R. Chintada, R. Rau, and O. Goksel, "Nonlinear characterization of tissue viscoelasticity with acoustoelastic attenuation of shear-waves," *arXiv preprint arXiv:2002.12908*, 2020.

[10] S. Catheline, J.-L. Gennisson, G. Delon, M. Fink, R. Sinkus, S. Abouelkaram, and J. Culioli, "Measurement of viscoelastic properties of homogeneous soft solid using transient elastography: An inverse problem approach," *The Journal of the Acoustical Society of America*, vol. 116, no. 6, pp. 3734–3741, 2004.

[11] S. Kazemirad, S. Bernard, S. Hybois, A. Tang, and G. Cloutier, "Ultrasound shear wave viscoelastography: Model-independent quantification of the complex shear modulus," *IEEE transactions on ultrasonics, ferroelectrics, and frequency control*, vol. 63, no. 9, pp. 1399–1408, 2016.

[12] S. Bernard, S. Kazemirad, and G. Cloutier, "A frequency-shift method to measure shear-wave attenuation in soft tissues," *IEEE transactions on ultrasonics, ferroelectrics, and frequency control*, vol. 64, no. 3, pp. 514–524, 2016.

[13] E. Budelli, J. Brum, M. Bernal, T. Deffieux, M. Tanter, P. Lema, C. Negreira, and J.-L. Gennisson, "A diffraction correction for storage and loss moduli imaging using radiation force based elastography." *Physics in medicine and biology*, vol. 62, no. 1, pp. 91–106, 2017.

[14] I. Z. Nenadic, M. W. Urban, S. Aristizabal, S. A. Mitchell, T. C. Humphrey, and J. F. Greenleaf, "On lamb and rayleigh wave convergence in viscoelastic tissues," *Physics in Medicine & Biology*, vol. 56, no. 20, p. 6723, 2011.

[15] I. Z. Nenadic, M. W. Urban, M. Bernal, and J. F. Greenleaf, "Phase velocities and attenuations of shear, lamb, and rayleigh waves in plate-like tissues submerged in a fluid (l)," *The Journal of the Acoustical Society of America*, vol. 130, no. 6, pp. 3549–3552, 2011.

[16] X. Zhang, B. Zhou, S. Kalra, B. Bartholmai, J. Greenleaf, and T. Osborn, "An ultrasound surface wave technique for assessing skin and lung diseases," *Ultrasound in medicine & biology*, vol. 44, no. 2, pp. 321–331, 2018.

[17] P. Garteiser, S. Doblas, J.-L. Daire, M. Wagner, H. Leitao, V. Vilgrain, R. Sinkus, and B. E. Van Beers, "Mr elastography of liver tumours: value of viscoelastic properties for tumour characterisation," *European radiology*, vol. 22, no. 10, pp. 2169–2177, 2012.

[18] I. Z. Nenadic, B. Qiang, M. W. Urban, H. Zhao, W. Sanchez, J. F. Greenleaf, and S. Chen, "Attenuation measuring ultrasound shearwave elastography and in vivo application in post-transplant liver patients," *Physics in Medicine & Biology*, vol. 62, no. 2, p. 484, 2016.

[19] T. Loupas, J. Powers, and R. W. Gill, "An axial velocity estimator for ultrasound blood flow imaging, based on a full evaluation of the doppler equation by means of a two-dimensional autocorrelation approach," *IEEE Trans Ultrasonics, Ferroelectrics, and Frequency Control*, vol. 42, no. 4, pp. 672–688, 1995.

[20] C. Strobbia and S. Foti, "Multi-offset phase analysis of surface wave data (mopa)," *Journal of Applied Geophysics*, vol. 59, no. 4, pp. 300–313, 2006.

[21] J. Achenbach, *Wave propagation in elastic solids*. Elsevier, 2012.

[22] M. Bernal, F. Chamming?s, M. Couade, J. Bercoff, M. Tanter, and J.-L. Gennisson, "In vivo quantification of the nonlinear shear modulus in breast lesions: feasibility study," *IEEE transactions on ultrasonics, ferroelectrics, and frequency control*, vol. 63, no. 1, pp. 101–109, 2016.

[23] C. F. Otesteanu, B. R. Chintada, M. Rominger, S. Sanabria, and O. Goksel, "Spectral quantification of nonlinear elasticity using acousto-elasticity and shear-wave dispersion." *IEEE transactions on ultrasonics, ferroelectrics, and frequency control*, 2019.

[24] B. R. Chintada, R. Rau, and O. Goksel, "Acoustoelasticity analysis of shear waves for nonlinear biomechanical characterization of oil-gelatin phantoms," in *2019 IEEE International Ultrasonics Symposium (IUS)*. IEEE, 2019, pp. 423–426.